

## PECULIARITIES IN THE FOREST FIRE DETECTION UNDER CONDITIONS OF BROKEN CLOUDS

V.G. Astafurov

*Institute of Atmospheric Optics,  
Siberian Branch of the Russian Academy of Sciences, Tomsk  
Tomsk State University of Control Systems and Radioelectronics*

*Received November 27, 1998*

*Accepted November 27, 1998*

*A numerical simulation technique is used to continue the study of statistical characteristics of radiometer-recorded power of upward IR radiation emitted by a fire and its background in the wavelength intervals 3.55–3.93 and 10.3–11.3  $\mu\text{m}$ . Mostly the attention is focused on the probability density of the recorded power and on its approximations. The Neumann-Pearson test and a closed numerical experiment are used to estimate the detection probability of the fires of different sizes. The results obtained illustrate the efficiency of the proposed approach.*

### INTRODUCTION

Early detection of forest fires allows a considerable reduction of the number of large fires and makes their extinguishing less expensive. A tendency for an increase in the area of fire-damaged forests has been noted in Russia in recent years.<sup>1</sup> For instance, in 1998 about 2 million hectares of forests were damaged by fires in Khabarovsk region, and tens of thousands of hectares in Sakhalin. This increase is primarily due to the growth of anthropogenic load in the West Siberia, Krasnoyarsk region, Baikal region, and Far East. The anthropogenic factors are responsible for about 80% of all fires,<sup>2</sup> and thunderstorms for 20 to 30% of fires, depending on the region.

The forest fires can be detected using different indications: elevated temperature, emission of gaseous products of combustion ( $\text{H}_2$ ,  $\text{CO}$ ,  $\text{CO}_2$ ,  $\text{CH}_4$ ,  $\text{C}_2\text{H}_2$ , nonsaturated hydrocarbons) into the atmosphere, smoke plumes, and color changes of fire-damaged forest areas.<sup>2,3</sup> Multichannel satellite-borne radiometers provide real-time obtaining of information on a cloud field, physical state of the atmosphere and underlying surface on a global scale. In particular, the surface temperature measurements make it possible to detect, by the upward going IR radiation the high-temperature anomalies, the appearance of which may be caused by the forest fires. Authors of Ref. 4 declare that the infrared measurements in the 3.55–3.93  $\mu\text{m}$  channel of the Advanced Very High Resolution Radiometer (AVHRR)<sup>5</sup> installed onboard the NOAA meteorological satellite can detect the flaming zones (FZs) measuring 10×10 m with the temperature  $T \sim 800$  K, or smoldering zones as small as 30×30 m with  $T \sim 500$  K.

This paper is a continuation of an earlier work on fire detection under conditions of the cloudy atmosphere.<sup>6</sup> The frequency of occurrence of the clear

sky conditions above the territory of Siberia and Far East is only from 10 to 20% in the March–May period and about 10% from July to August.<sup>7</sup> The mean cloud amount in these regions ranges from 4 to 5 in the March–May period and 6 from July to August. The mean frequency of occurrence of the cloud amount of 1–4 is about 28% in the March–May period and 25% in June–July. For the cloud amount of 5–7 these values are 26 and 35%, while for cloud amount of 8–10 they lie in the ranges of 10–20 and 30–40%, respectively. It should be also noted that almost every fifth fire is caused by a thunderstorm, that is its origin and development are associated with clouds. Thus, in the general case the task of detecting fires must be achieved for conditions of cloudy skies. The moderate cloud amount from 1 to 7, most frequently occurring, is therewith of the greatest interest.

### FORMULATION OF THE PROBLEM AND TECHNIQUE OF COMPUTATION

Figure 1 presents a scheme of fire detection using the IR radiometer located at the height  $H_0$ .

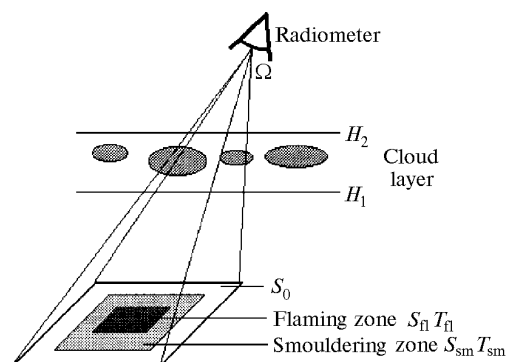


FIG. 1. Geometry of fire detection under conditions of broken clouds.

A possibility of detecting fires under broken clouds strongly depends on the existence of gaps in the clouds and optically thin cloud edges within the optical detector's field of view (FOV). Following Ref. 8, we will use the term "broken clouds" for a field of cumulus clouds with stochastic geometry and determinate internal structure. A cloud layer occupies the height interval  $[H_1, H_2]$ , within which the total extinction coefficient at altitude  $z$  is

$$\alpha_{\Sigma}(z, \lambda) = \alpha(z, \lambda) + \chi(\mathbf{r}) \alpha_c(\lambda). \quad (1)$$

Here  $\alpha(z, \lambda)$  is the coefficient of aerosol and gas extinction;  $\alpha_c(\lambda)$  is the cloud extinction coefficient; and  $\chi(\mathbf{r})$  is the indicator field:

$$\chi(\mathbf{r}) = 1, \mathbf{r} \in \Theta \text{ and } \chi(\mathbf{r}) = 0, \mathbf{r} \notin \Theta,$$

where  $\Theta$  is a random set of points at which the cloud matter occurs. The power recorded with a radiometer in the wavelength range  $\Delta\lambda$  is determined by the equation

$$p(\xi, \Delta\lambda) = \int_{\Omega} d\omega \int_{S_R^*} d\rho \int_{\Delta\lambda} d\lambda k(\lambda) I(\rho, \omega, \lambda), \quad (2)$$

where  $\xi$  is the sighting angle;  $S_R^*$  is the surface of the radiometer receiving aperture with the area  $S_R$ ;  $\Omega$  is the radiometer FOV angle;  $k(\lambda)$  is the transmission coefficient of optical filter at the wavelength  $\lambda$ ;  $I(\rho, \omega, \lambda)$  is the intensity of the upward going thermal radiation at the point  $\rho \in S_R^*$  in the direction of the unit vector  $\omega$ . As in Ref. 6, we assume, that the clouds do not scatter and the underlying surface is characterized by the temperature distribution  $T_s(x, y)$  and the emissivity  $\varepsilon[\lambda, T_s(x, y)]$ .

The intensity of the upward going thermal radiation at the height  $H_0$  is<sup>9</sup>:

$$\begin{aligned} I(\rho, \omega, \lambda) &= \varepsilon(\lambda, T_s(x, y)) B_{\lambda}(T_s(x, y)) \times \\ &\times \exp\left(-\frac{1}{\mu} \int_0^{H_0} \alpha_{\Sigma}(s, \lambda) ds\right) + \int_0^{H_0} B_{\lambda}(T(z)) \times \\ &\times \exp\left(-\frac{1}{\mu} \int_z^{H_0} \alpha_{\Sigma}(s, \lambda) ds\right) \frac{\alpha_{\Sigma}(z, \lambda)}{\mu} dz, \end{aligned} \quad (3)$$

where  $b_{\lambda}(T_s)$  is the Planck function;  $\mu = \cos \xi$ ;  $x = x(\omega, H_0)$ ;  $y = y(\omega, H_0)$ ; and  $T(z)$  is the temperature at the height  $z$ . Equation (3) does not take into account a contribution from surface-reflected solar radiation, although it may be significant in the wavelength range from 3.55 to 3.93  $\mu\text{m}$  in the case of strongly reflecting vegetation.<sup>10</sup> The radiation temperature  $T_R$  is determined from a solution of the equation

$$p(\xi, \Delta\lambda) / (\Omega S_R) = \int_{\Delta\lambda} B(T_R, \lambda) d\lambda. \quad (4)$$

As seen from Eq. (4),  $T_R$  characterizes some mean temperature of the surface area, within the radiometer

FOV, allowing for the effects of the cloudy atmosphere.

Investigation of fluctuations of the IR radiation, emitted by a fire and its background and recorded with the radiometer, is a basis for constructing the statistical criteria for fire detection. Under conditions of cloudy atmosphere, the fluctuations of power  $p(\xi, \Delta\lambda)$  result from (a) fluctuations of the total extinction coefficient  $\alpha_{\Sigma}(z, \lambda)$ ; (b) fluctuations of the air and surface temperature  $T(z)$  and  $T_s(x, y)$ ; and (c) fluctuations of the surface emissivity  $\varepsilon(\lambda, T_s(x, y))$ . However, here, as in Ref. 6, we account for only the dominating fluctuations, i.e.,  $\alpha_{\Sigma}(z, \lambda)$  caused by the stochastic geometry of a cloud field (the second term in Eq. (3)) and neglect the other ones.

The statistical characteristics of  $p(\xi, \Delta\lambda)$  and  $T_R$  are being sought using the numerical simulation technique described in detail in Ref. 6. The magnitude of  $\alpha_c(\lambda)$  corresponds to the model cloud  $C_1$ . Realizations of a cloud field are generated by means of the Poisson flux of points corresponding to the cloud base centers located at the height  $H_1 = 1$  km. Clouds are approximated by truncated inverted paraboloids of rotation. The height of a cloud is equal to its base diameter and it is considered to be a random quantity with the exponential distribution function.<sup>8</sup> For each realization of a cloud field we calculate the power  $p(\xi, \Delta\lambda)$  and the corresponding radiation temperature  $T_R$  using equation (4).

## THE CALCULATED RESULTS AND THEIR DISCUSSION

The occurrence of a fire within the radiometer FOV causes an increase in the radiation temperature  $T_R$  by  $\langle \Delta T_R \rangle$ , which depends on the temperature distribution in the fire zone and absorption of IR radiation in the spectral range under consideration. In calculations we used the simplest model of the fire consisting of two zones (Fig. 1): the smouldering zone with a constant temperature  $T_{sm}$  and the area  $S_{sm}$ , where the intense burning is already over, and the fire zone itself (FZ) with the enhanced temperature  $T_{fl}$  and the area  $S_{fl}$ ; beyond the burning area, the surface temperature is  $T_0$ . The relative size of the fire zones is given by two parameters:

$$d_1 = S_{sm}/S_0 \quad \text{and} \quad d_2 = S_{fl}/S_0,$$

where  $S_0$  is the total area of the surface within the radiometer FOV. All calculations were made assuming the following values of the parameters:  $H_0 = 850$  km,  $\Omega = 1.88 \cdot 10^{-6}$  sr,  $\xi = 0$ ,  $T_{fl} = 1000$  K,  $T_{sm} = 300$  K,  $\varepsilon = 1$ , the spectral ranges of 3.55–3.93 and 10.3–11.3  $\mu\text{m}$  that fall into the atmospheric transmission windows and correspond to the third and the fourth channels of the AVHRR radiometer.<sup>5</sup> The first spectral range coincides with the range of the surface emitting maximum at the characteristic temperature of the forest fires of 800–1000 K. The second range includes the spectral maximum of the underlying surface emission what allows an elimination of noise caused by the Earth surface

inhomogeneity.<sup>3</sup> Altitude profiles of the aerosol absorption coefficient are taken from Ref. 11. The transmission function for the ranges of the molecular absorption chosen is calculated for conditions of mid-latitude summer. The computational method is described in Ref. 12; the procedures for computation have been kindly afforded by K.M. Firsov.<sup>12</sup>

The radiometer measures the surface temperature with the spatial resolution  $S_0$  ( $S_0 \approx 1$  km when sounding in the nadir direction). Therefore, some equivalent temperature  $T^*$  of the entire area within the radiometer FOV is assigned to the FZ with the given temperature distribution. The dependence of  $T^*$  on relative size of the smouldering zone  $d_1$  at a fixed size of the burning zone under clear-sky conditions is presented in Fig. 2.

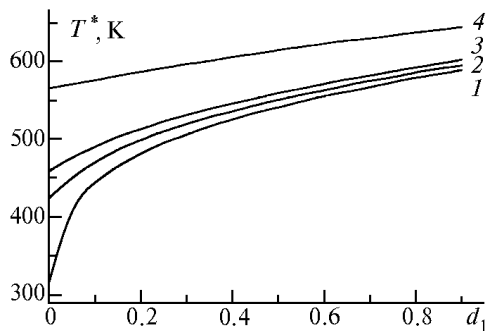


FIG. 2. Dependence of equivalent surface temperature  $T^*$  on relative size of the smouldering zone in the wavelength range of 3.55–3.93  $\mu\text{m}$  for different sizes of the burning zone:  $d_2 = 10^{-4}$  (1), 0.005 (2),  $10^{-2}$  (3), and 0.05 (4).

The results obtained illustrate high sensitivity of the IR radiation detector to high-temperature anomalies in the underlying surface in the 3.55–3.93  $\mu\text{m}$  spectral range. For instance, the FZ of 100  $\text{m}^2$  area and 1000 K temperature causes  $T^*$  to

increase from 300 to 315 K. Unfortunately, the AVHRR radiometers have a threshold of saturation which, depending on the satellite series, ranges from 322 (NOAA-7) to 331 K (NOAA-10),<sup>3</sup> thus seriously complicating determination of the FZ sizes as well as the fire distinguishing against a strong background noise. Figure 3 shows the dependence of the mean radiation-temperature gain  $\langle \Delta T_R \rangle$  and relative standard deviation  $\delta_T = \sqrt{D(T_R)} / \langle \Delta T_R \rangle$  on the cloud amount  $N$ . The larger is  $N$ , the less is  $\langle \Delta T_R \rangle$ . A decrease of  $\langle \Delta T_R \rangle$  with  $N$  growth is caused by higher probability of fires screening by clouds. Calculations of the dependence of the moments  $p(\xi, \Delta\lambda)$  on the cloud amount are presented and discussed in Ref. 6.

The probability density  $f(p)$  is the most perfect statistical characteristic of  $p(\xi, \Delta\lambda)$ . Figure 4 presents the histograms calculated for  $v(p^*)$ . Here  $p^* = p(\xi, \Delta\lambda) / p_0(\xi, \Delta\lambda)$ , where  $p_0(\xi, \Delta\lambda)$  is the power recorded under clear sky conditions at the surface temperature  $T_s = T_0$ . Obviously, in the absence of fires, and at  $N = 0$ ,  $f_0(p) = \delta(1 - p/p_0)$ , where  $\delta(x)$  is the delta-function.

Under the overcast  $f_0(p) = \delta(1 - p/p_{\min})$ , where  $p_{\min}$  is the minimum recorded power of the upward IR radiation emitted by the atmosphere above the cloud. The histograms for  $v_0(p^*)$  shown in Figs. 4a and b illustrate an intermediate situation. Noteworthy, at  $N = 0.5$  the histogram "width" is maximum because of the largest variance of the IR radiation power in this case.

When a fire occurs within the radiometer FOV,  $v_0(p^*)$  becomes bimodal (Figs. 4c and d). The first peak of  $v_0(p^*)$  at  $p^* < 1$  is due to the surface area emission at the temperature  $T_0$ , while the second one is caused by a high-temperature anomaly. Based on the results obtained, we may conclude, that the earlier proposed approximation<sup>6</sup> of the probability density  $f(p)$  by the gamma distribution is possible only in the absence of fires within the radiometer FOV.

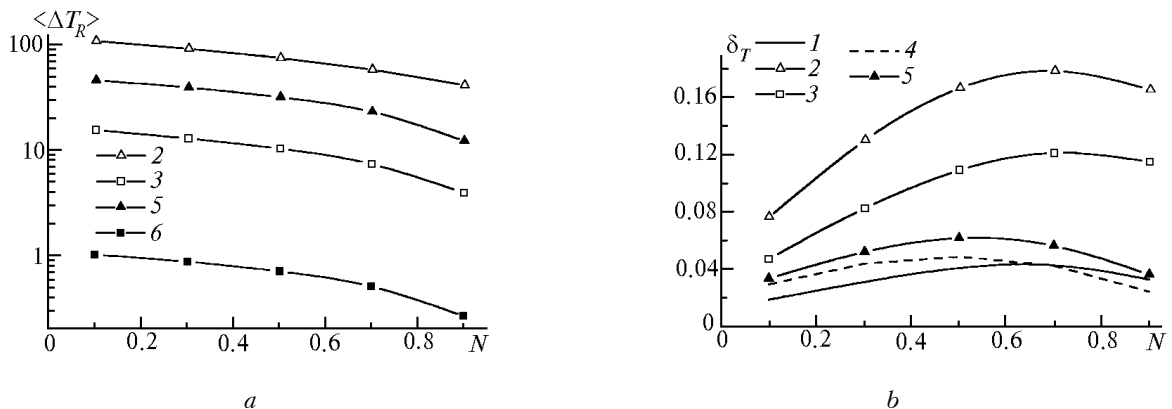


FIG. 3. The temperature gain  $\langle \Delta T_R \rangle$  (a) and relative standard deviations of temperature  $\delta_T$  (b) as functions of the cloud amount  $N$  for the spectral regions of 3.55–2.93  $\mu\text{m}$  (curves 1, 2, 3) and 10.3–11.3  $\mu\text{m}$  (curves 4, 5, 6);  $d_1 = 0$ ,  $d_2 = 0$  (no fire) (curves 1, 4);  $d_1 = 2.4 \cdot 10^{-2}$ ,  $d_2 = 2.5 \cdot 10^{-3}$  (curves 2, 5);  $d_1 = 0$ ,  $d_2 = 6.3 \cdot 10^{-4}$  (curves 3, 6).

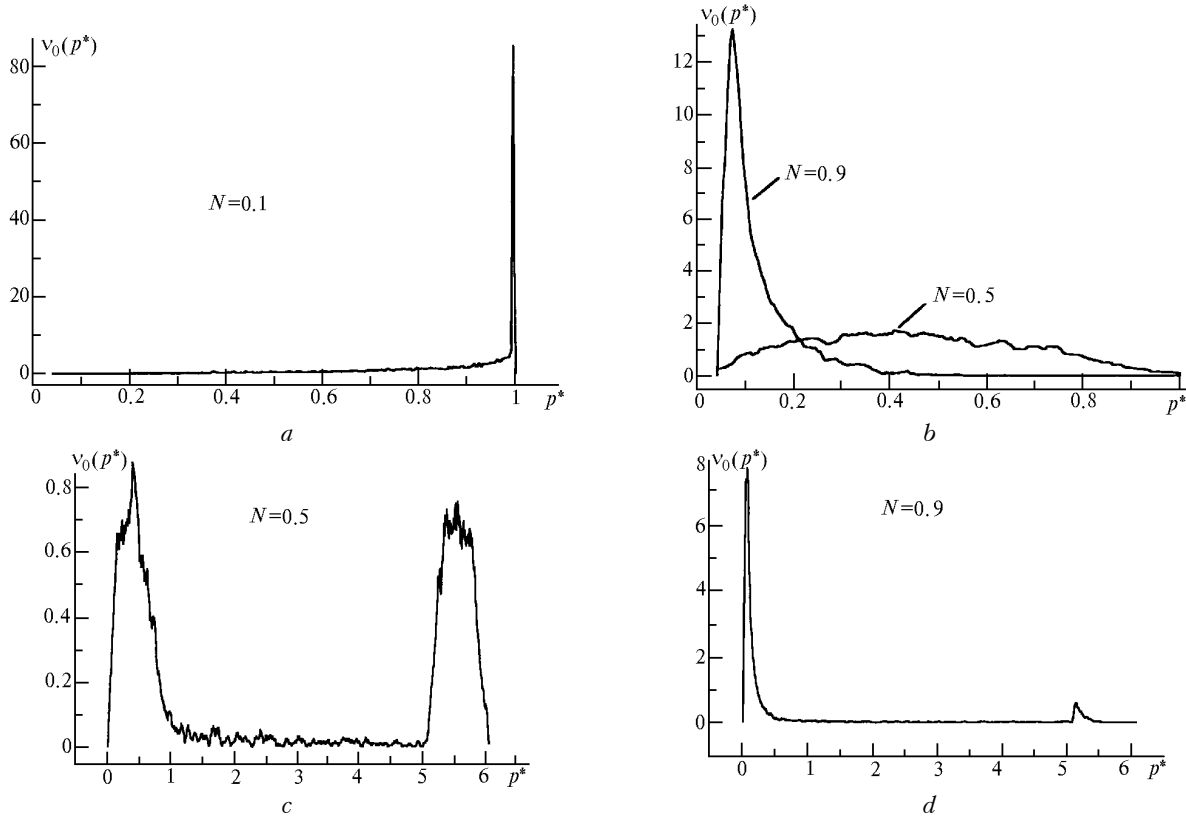


FIG. 4. Histograms of the normalized power of radiation coming from the background (a, b) and the total radiation coming from the background and FZ with the relative sizes  $d_1 = 0$  and  $d_2 = 6.3 \cdot 10^{-4}$  (c, d) in the spectral range of 3.55–3.93  $\mu\text{m}$ .

Now we consider the case of a point FZ and derive an approximate expression for the probability density  $f(p)$ . The radiometer records the total power  $p = p_{s,a} + p_{fl}$ , where  $p_{s,a}$  is the power of the IR radiation from the atmosphere and the surface with  $T_s = T_0$ , and  $p_{fl}$  is that from the FZ. We assume that the FZ is a point area and clouds have no optically thin edges. A direction towards FZ within the radiometer FOV is denoted by the unit vector  $\mathbf{l}$ . This direction is covered with clouds with the probability  $n(\mathbf{l})$ . For isotropic cloud fields, this probability is  $n(\xi_0)$ , where  $\xi_0$  is an angle between the line of sight to the fire and the nadir direction recorded under clear skies at the temperature of the underlying surface  $T_s = T_0$  (Fig. 5). Obviously, at  $\xi_0 = 0$ , the probability of screening the line of sight with clouds  $n(0) = N$ . Since  $\Omega \ll 1$ , then  $\xi \approx \xi_0$ . The probability density  $f_1(p_{fl})$  is given as

$$f_1(p_f) = n(\xi) \delta(p_{fl}) + (1 - n(\xi)) \delta(p_{fl} - p_{f0}),$$

where  $p_{f0}$  is the power of the fire recorded under clear sky conditions. Let  $f_2(p_{s,a})$  be the probability density  $p_{s,a}$  under cloudy skies. With  $p_{s,a}$  and  $p_{fl}$  assumed to be independent, we find the convolution of  $f_1(p_{fl})$  and  $f_2(p_{s,a})$ :

$$f(p) = n(\xi) f_2(p) + (1 - n(\xi)) f_2(p - p_{f0}).$$

It is seen from this expression that  $f(p)$  has two peaks; the relation between them is determined by the probability  $n(\xi)$ ; their shapes are similar and have the form of  $f_2(p)$ . A slight deformation of the peaks of  $v(p^*)$  in Fig. 4c can be explained by a violation of the assumption that  $p_{s,a}$  and  $p_{fl}$  are independent, possibly because the FZ and the surface are partially screened by one and the same cloud.

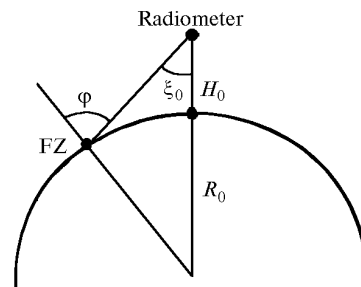


FIG. 5. Geometrical parameters:  $\xi_0$  is the sighting angle toward a point fire and  $\phi$  is the zenith angle.

When the gamma-distribution is used to approximate  $f_2(p)$ , the probability density becomes

$$f(p) = \frac{\exp(-p/\eta)}{\Gamma(\nu + 1) \eta^{\nu+1}} \{n(\xi) p^\nu - h(p - p_{f0}) (1 - n(\xi)) (p - p_{f0})^\nu \exp(-p_{f0}/\eta)\},$$

where  $\Gamma(x)$  is the gamma-function;  $h(x)$  is the step function of the a unit jump:

$$h(x) = \begin{cases} 1, & x \geq 0, \\ 0, & x < 0; \end{cases}$$

and the parameters  $\nu$  and  $\eta$  are given as

$$\nu = \frac{\langle p_{s,a} \rangle}{D(p_{s,a})} - 1, \quad \eta = \frac{D(p_{s,a})}{\langle p_{s,a} \rangle}.$$

The dependences of the mean power  $\langle p_{s,a} \rangle$  and variance  $D(p_{s,a})$  on the cloud amount  $N$  at  $\xi = 0$  may be found in Ref. 6.

The probability of screening the line of sight with clouds  $n(\varphi)$  as a function of the FZ zenith angle (see Fig. 5) for different models of a cloud field was considered in Ref. 13, where one can also find a comparative analysis of the obtained results. A comparison of the theoretical and experimental functions  $n(\varphi)$  is presented in Ref. 14. It follows from these results that the most acceptable relationship for  $n(\varphi)$  calculation is as follows:

$$n(\varphi) = N \exp[-N(\Psi(\varphi) - 1)] - \exp[-N(\Psi(\varphi) - 1)] + 1,$$

where

$$\Psi(\varphi) = \frac{1}{2} + \frac{1}{2} \operatorname{erf} \left[ \frac{\cot \varphi}{\sigma_{z'} \sqrt{2}} \right] + \frac{\sigma_{z'}}{\sqrt{2\pi} \cot \varphi} \exp \left[ -\frac{\cot^2 \varphi}{2 \sigma_{z'}^2} \right];$$

$\sigma_{z'}^2$  is the variance of the derivative of a standard random surface, and  $\operatorname{erf}(x)$  is the error function. Based on the sky photographs, it was found<sup>11</sup> that  $\sigma_{z'}^2$  increases insignificantly with cloud amount, on the average  $\sigma_{z'}^2 = 1.4$ . It is also shown that  $n(\varphi)$  essentially increases starting from a zenith angle of  $50^\circ$ . It could be shown that the  $\xi$  and  $\varphi$  angles depicted in Fig. 5 are related as

$$\varphi = \arcsin [(1 + H_0/R_0) \sin \xi],$$

where  $R_0$  is the radius of the Earth. For the maximum sighting angle of the AVHRR radiometer  $\xi = 55.4^\circ$ , the corresponding zenith angle is  $\varphi = 68.9^\circ$ .

The  $\nu(p^*)$  histograms can be used for calculating the probabilities detecting the FZs of different size. The Neumann-Pearson test is suggested for this purpose.<sup>6</sup> The detection algorithm compares the radiometer-recorded power  $p(\xi, \Delta\lambda)$  with the threshold  $u_\alpha$ , determined from the given false alarm probability  $\alpha$  by the equation

$$\alpha = \int_0^{u_\alpha} f_0(p) dp,$$

where  $f_0(p)$  is the probability density of the background. In the calculations we used the corresponding estimate of  $\nu_0(p^*)$  instead. The magnitude of  $\alpha$  characterizes the probability of an incorrect decision on FZ presence within the radiometer FOV. The probability of the FZ detection is

$$1 - \beta = \int_{u_\alpha}^{+\infty} f(p) dp.$$

Shown in Table I are the probabilities for detection of different FZs with  $d_1 = 0$  calculated for the wavelength range of 3.55–3.93  $\mu\text{m}$ . At  $\alpha = 0$  the threshold  $u_\alpha = p_0(\xi, \Delta\lambda)$ , in which case the optical detector records only those FZs within its field of view, for which the fixed power exceeds the background level  $p_0(\xi, \Delta\lambda)$  corresponding to clear-sky conditions. In some very few cases the detection is possible through optically thin cloud edges. For this reason, the probability of detecting the FZs of  $25 \times 25 \text{ m}^2$  area is  $1 - \beta = 0.544$  at  $N = 0.5$ , that is higher than the 0.5 probability of falling within the cloud gaps. Assuming even small non-zero  $\alpha$ , we gain in the detection efficiency, almost without loss in its quality. This is clearly seen for the cloud amount  $N = 0.9$ .

TABLE I. Probability of detecting FZ of the temperature  $T_{\text{fl}} = 1000 \text{ K}$  using the Neumann-Pearson test.

| Area<br>(size) of FZ             | $\alpha$ | Detection probability |           |           |
|----------------------------------|----------|-----------------------|-----------|-----------|
|                                  |          | $N = 0.5$             | $N = 0.7$ | $N = 0.9$ |
| 625 m <sup>2</sup><br>(25 × 25)  | 0.00     | 0.544                 | 0.342     | 0.162     |
|                                  | 0.01     | 0.551                 | 0.362     | 0.221     |
|                                  | 0.02     | 0.555                 | 0.374     | 0.241     |
|                                  | 0.05     | 0.565                 | 0.397     | 0.273     |
| 1250 m <sup>2</sup><br>(25 × 50) | 0.00     | 0.568                 | 0.386     | 0.213     |
|                                  | 0.01     | 0.575                 | 0.407     | 0.265     |
|                                  | 0.02     | 0.582                 | 0.418     | 0.283     |
|                                  | 0.05     | 0.591                 | 0.441     | 0.311     |
| 1875 m <sup>2</sup><br>(25 × 75) | 0.00     | 0.593                 | 0.420     | 0.256     |
|                                  | 0.01     | 0.599                 | 0.439     | 0.309     |
|                                  | 0.02     | 0.602                 | 0.448     | 0.325     |
|                                  | 0.05     | 0.611                 | 0.470     | 0.354     |
| 2500 m <sup>2</sup><br>(50 × 50) | 0.00     | 0.598                 | 0.430     | 0.266     |
|                                  | 0.01     | 0.603                 | 0.447     | 0.319     |
|                                  | 0.02     | 0.608                 | 0.457     | 0.337     |
|                                  | 0.05     | 0.618                 | 0.478     | 0.366     |

The results presented are preliminary due to a number of simplifying approximations. Further investigation should be directed to constructing a complete statistical model of the background taking into account the noise due to solar radiation scattered by clouds as well as the fluctuations of surface temperature and emissivity. The radiation emitted by the background and the FZ and recorded with a radiometer has distinctly different spectral dependence. Multispectral measurements should provide very important information on the fires and thus make their detection more reliable. These investigations should result in the algorithms for the FZs identifying with the present and future radiometers at any time of day

and night by outgoing IR radiation against the noise background.

#### ACKNOWLEDGMENTS

The problem of fire detection under cloudy skies was first formulated by Doctor G.A. Titov. The author is grateful to G.A. Titov for his constant attention to this work and helpful discussions of obtained results. These calculations employ his algorithm of simulating the realizations of a cloud field, based on the Poisson flux of points. Additional thanks are to Dr. K.M. Firsov for the computer codes for calculation of the transmission functions he has kindly presented at our disposal.

#### REFERENCES

1. V.G. Sokolovskii, *Environmental Conditions in the USSR in 1988* (Goskompriroda SSSR, Moscow, 1989), 203 pp.
2. A.M. Grishin, *Physics of Forest Fires* (Tomsk State University Publishing House, Tomsk, 1994), 218 pp.
3. T.B. Kondarin and E.V. Ovchinnikova, *Issled. Zemli iz Kosmosa*, No. 4, 51–57 (1995).
4. Y.J. Kaufman and C.J. Tucker, *J. Geophys. Res.* **95**, No. D7, 9927–9939 (1990).
5. L. Lauritson, G.J. Nelson, and F.W. Porto, *Data Extraction and Calibration of "Tiros-N"/NOAA Radiometers NESS-107, Technical Memorandum* (Washington, D.C., 1979), 58 pp.
6. V.G. Astafurov and G.A. Titov, *Atmos. Oceanic Opt.* **9**, No. 5, 409–414 (1996).
7. Yu.L. Matveev, L.T. Matveev, and S.A. Soldatenko, *Global Cloud Field* (Gidrometeoizdat, Leningrad, 1986), 280 pp.
8. V.E. Zuev and G.A. Titov, *Atmospheric Optics and Climate* (Izd. Spectr, Tomsk, 1996), 271 pp.
9. Kuo-Nan Liou, *Fundamentals of Atmospheric Radiation Processes* (Gidrometeoizdat, Leningrad, 1984), 376 pp.
10. M.S. Malkevich, *Optical Satellite Observations of the Atmosphere* (Nauka, Moscow, 1973), 303 pp.
11. G.M. Krekov and R.F. Rakhimov, *Optical Models of Atmospheric Aerosol* (Publishing House of Tomsk Affiliate of Siberian Branch of the Academy of Sciences of USSR, Tomsk, 1986), 294 pp.
12. K.M. Firsov and T.Yu. Chesnokova, *Atmos. Oceanic Opt.* **11**, No. 4, 356–360 (1998).
13. O.A. Avaste, Yu.R. Mullamaa, Kh.Yu. Niilisk, and M.A. Sulev, *Heat Exchange in the Atmosphere* (Nauka, Moscow, 1972), pp. 134–139.
14. Yu.R. Mullamaa, ed., *Stochastic Structure of Cloud and Radiation Fields* (Institute of Physics and Astronomy, Estonian Academy of Sciences, Tartu, 1972), 282 pp.